

Effective magnetic susceptibility of suspensions

Kunlun Bai, Aparna Nair-Kanneganti, Aubrey Wahl, and Florian Carle
Department of Mechanical Engineering and Materials Science, Yale University, New Haven, CT 06511, USA

Joshua Casara
School of Natural Sciences, University of California, Merced, CA 95343, USA

Eric Brown*
*Department of Mechanical Engineering and Materials Science,
Yale University, New Haven, CT 06511, USA and
School of Natural Sciences, University of California, Merced, CA 95343, USA*
(Dated: May 8, 2019)

We characterize how suspensions of magnetic particles in a liquid respond to a magnetic field in terms of the effective magnetic susceptibility χ_{eff} using inductance measurements. We test a model that predicts how χ_{eff} varies due to demagnetization, as a function of sample aspect ratio, particle packing fraction, and particle aspect ratio [1]. For spherical particles or cylindrical particles aligned with external magnetic field, the model can be fitted to the measured data with agreement within 17%. However, we find that the random alignment of particles relative to the magnetic field plays a role, reducing χ_{eff} by a factor of 3 in some cases, which is not accounted for in models yet. While suspensions are predicted to have χ_{eff} that approach the particle material susceptibility in the limit of large particle aspect ratio, instead we find a much smaller particle aspect ratio where χ_{eff} is maximized. A prediction that χ_{eff} approaches the bulk material susceptibility in the limit of the packing fraction of the liquid-solid transition also fails. We find χ_{eff} no larger than about 4 for suspensions of iron particles.

I. INTRODUCTION

Suspensions of magnetic particles in a liquid can be controlled by an applied magnetic field, a property that is taken advantage of for example in the fields of ferrohydrodynamics [2] and magnetorheology [3]. The parameter that directly controls the force applied by a magnetic field in these cases is the effective magnetic susceptibility χ_{eff} . If the suspensions are also conducting, magnetohydrodynamic effects can occur, such that a magnetic field can in principle be generated by the conducting fluid flow, and the magnetic field can deflect the conducting flow via a Lorentz force, effects whose magnitude scales with $1 + \chi_{eff}$ [4–6]. While these phenomena are not easily achieved with known fluids – where pure conducting liquids generally have a magnetic susceptibility $\chi \ll 1$ – there is potential that if a material can be designed with large enough $\chi_{eff} \gtrsim 1$, these phenomena could be more easily observed on a laboratory or device scale of order 10 cm [7]. Our goal is to determine how the effective magnetic susceptibility χ_{eff} depends on the particle properties of suspensions. In particular, we would like to obtain larger values of χ_{eff} to make such suspensions useful for producing magnetohydrodynamic phenomena on the laboratory scale.

The effective susceptibility χ_{eff} is defined by the proportionality $\chi_{eff} = \phi M / H_{app}$, where H_{app} is an externally applied magnetic field, M is the magnetization per unit volume of magnetic material, and ϕ is the volume

fraction of the magnetic particles. Note that the factor of ϕ in the expression differs from traditional definitions in pure materials where susceptibility is defined per unit volume of magnetic material, as a pure material is 100% magnetic material. Instead we define χ_{eff} as susceptibility per unit volume of sample, since we are interested in the force from an applied magnetic field on the sample as a whole. For linear magnetic materials χ_{eff} is independent of H_{app} , in practice this tends to be the case for small H_{app} before the magnetization begins to saturate.

Locally, the magnetic susceptibility $\chi = M/H$ is considered a bulk material property depending on the local magnetic field H . In contrast, χ_{eff} as a macroscopic parameter can be much smaller than χ due to demagnetization, an effect in which the induced magnetic dipole creates an additional magnetic field DM (where D is called the demagnetization factor) that opposes H_{app} . The net magnetic field inside the material $H_{app} - DM$ that determines the net local magnetization M is less than H_{app} , resulting in χ_{eff} being smaller than χ . The effective susceptibility can then be written such that the demagnetization is a correction factor on the material susceptibility:

$$\frac{\phi}{\chi_{eff}} = \frac{1}{\chi} + D. \quad (1)$$

It is well-known for single-piece solid magnets, for example, that D depends on the shape of the magnet, in particular D is small in the limit of long, thin magnets aligned with the applied magnetic field, (in this limit χ_{eff} approaches the material susceptibility χ). For single-piece solids, unless the aspect ratio of the material is

* eric.brown@yale.edu

extremely large, $\chi_{eff} \ll \chi$ and to a good approximation $\chi_{eff} \approx \phi/D$. χ_{eff} has been calculated for many particle shapes [8]. For example, for a spherical particle $D = 1/3$, resulting in a maximum $\chi_{eff} \approx 3$ as long as $\chi \gg 3$. For such geometries with aspect ratio close to 1, the demagnetization effect can be considered a dominating factor determining χ_{eff} , rather than a small perturbation on the material susceptibility χ .

Demagnetization factors are less well-understood for systems of random arrangements of particles such as suspensions. With many particles, the demagnetization factor D can depend on geometries of both the particles and the sample as a whole, as well as positions and alignments of particles relative to each other and the applied magnetic field.

For example, in the magnetorheological effect, a suspension exposed to an applied magnetic field develops a yield stress. The magnitude of this yield stress scales roughly as the force of the induced dipole-dipole interaction between the particles in suspension, which is proportional to χ_{eff}^2 [3]. It has been observed that large-aspect ratio rod-shaped particles exhibit a larger yield stress than spherical particles, which was qualitatively attributed to the demagnetization effect [9]. However, this is not quantitatively understood, due to the lack of a model that relates this yield stress to χ_{eff} and the demagnetization effect.

For randomly packed spherical particles, it has been theoretically argued that the demagnetization factor is $D = \frac{1}{3} + \phi(D_g - \frac{1}{3})$, where D_g is the global demagnetization factor based on the geometry of the sample and ϕ is the volumetric packing fraction [10]. D_g was assumed to be the same as the demagnetization factor for a single particle of the same shape. A numerical calculation confirmed this model is a good approximation within 3% for a sample of randomly packed spherical particles for sample aspect ratios $\gamma_g = 0.5$ to 1, and packing fractions ϕ from 0.4 to 0.6 [11]. It remains to be seen how well the prediction holds over a wider parameter range, in particular at larger γ_g where χ_{eff} is expected to be larger.

A more general model takes advantage of the fact that exact expressions can be found for homogeneously magnetized ellipsoids of revolution to obtain an expression for ellipsoidal particles homogeneously dispersed in any non-magnetic medium (including suspensions) in which particles are aligned with each other and the external magnetic field [1]. This demagnetization factor is

$$D = D_p(1 - \phi) + D_g\phi \quad (2)$$

where D_p is the demagnetization factor of each particle (they are assumed to be identical). D_p may be different from the global demagnetization factor D_g , and so is an unknown function of particle geometry. An expression for χ_{eff} can be obtained by combining Eq. 1 and 2, which simplifies if demagnetization effects are as significant as they are for typical for single-piece ferromagnetic

materials in the limit where $\chi \gg \chi_{eff}$ to

$$\chi_{eff} \approx \frac{\phi}{D_p(1 - \phi) + D_g\phi}. \quad (3)$$

To our knowledge, it has not yet been tested whether this model captures the effects of different particle shapes on χ_{eff} – specifically there is no model or data on how D_p depends on particle aspect ratio or other parameters.

An alternate model designed for the limit of high packing fraction ϕ assumes that magnetic field lines tend to go from one ferromagnetic particle to another along regions of high susceptibility, and thus concentrate their density in paths along the shortest distances between particles [12]. It predicts that χ_{eff} diverges as the gaps between magnetic particles go to zero, approaching the material susceptibility χ , according to

$$\chi_{eff} = \frac{1}{1 - (\phi/\phi_c)^{1/3}} - 1, \quad (4)$$

while $\chi_{eff} \ll \chi$. The critical packing fraction ϕ_c physically corresponds to the liquid-solid transition where particles with no long-range repulsions just barely touch. While this model has been tested at low ϕ , it has not been tested at ϕ within 0.08 of the liquid-solid transition where the divergence would be expected to produce $\chi_{eff} \gg 1$ [12, 13], so it is not yet known if this divergence can be realized in suspensions.

In this manuscript, we test the above predictions for χ_{eff} for suspensions of cylindrical and spherical particles in cylindrical samples, by measuring χ_{eff} over a wide range of packing fraction ϕ up to ϕ_c , sample aspect ratio γ_g , and particle aspect ratio γ_p . The remainder of the manuscript is organized as follows. We first describe the suspensions used in Sec. II A. We describe the gradiometer we built to measure χ_{eff} in Sec. II B, and its calibrations in Secs. II C and II D. We test the linearity of the magnetic response of the suspensions in current and frequency in Sec. III A. Measurements of χ_{eff} as a function of ϕ , γ_g and γ_p are reported in Sec. III B. We use this to fit the demagnetization functions D_p and D_g from Eq. 2 as a function of aspect ratios γ_p and γ_g , respectively, in Sec. III C. Finally in Sec. III D, we vary particle aspect ratio γ_p in suspensions of randomly arranged particles to test whether particle alignment with the magnetic field plays an important role in χ_{eff} , an effect which was not accounted for in Eq. 2.

II. MATERIALS AND METHODS

A. Materials

We suspended iron particles (density 7.834 kg/m^3 and purity 99.5%) of mean diameter $29 \mu\text{m}$, where 90% of particle diameters are within the range $18\text{-}40 \mu\text{m}$, purchased from Chemicalstore.com. The particles are nearly

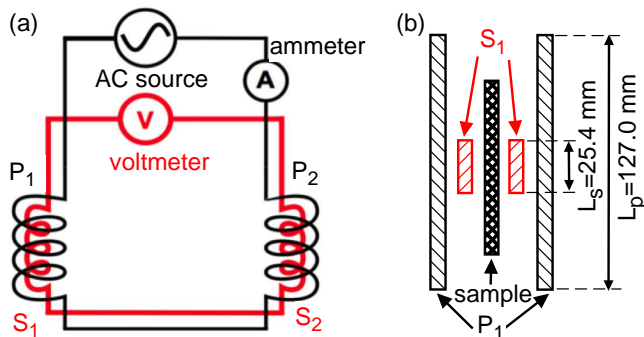


FIG. 1. (a) The circuit diagram of the gradiometer used to measure the effective susceptibility χ_{eff} of a sample based on the change in mutual inductance of a solenoid pair. (b) A diagram (not to scale) that shows a cross-section of the coils and sample.

spherical with a standard deviation of 4% in the diameter. We use these nearly spherical particles in experiments unless otherwise specified. The suspending liquid was a eutectic alloy of gallium and indium known as eGaIn, which was produced as described in [7]. We used a liquid metal for its potential in magnetohydrodynamic applications. The properties of the liquid metal are not expected to be important here, other than the effect of its conductivity 3.40×10^6 S/m [14] contributing to stronger eddy currents that could reduce χ_{eff} at high frequencies of applied alternating magnetic field (see Sec. III A). Samples were kept in an acid bath to prevent oxidation of the metals [7]. Dry granular samples were obtained by mixing the iron particles with non-magnetic sand.

In either case, the packing fraction ϕ was obtained by measuring masses of the constituent materials, and using density to convert to a packing fraction by volume of the magnetic material (iron) divided by the total volume taken up by the sample. In the case of dry granular samples, the total volume of the sample was measured directly as the volume taken up in the sample container, which includes some air.

B. Experimental setup

Measurements were taken using a gradiometer setup which consists of two pairs of inductor coils shown in Fig. 1. The gradiometer measures χ_{eff} of a material sample based on how it changes the mutual inductance between two surrounding coils P_1 and S_1 . The sample sits in a cylindrical tube which is placed inside the secondary coil S_1 , while coil S_1 is inside the primary coil P_1 . There is another nominally identical set of coils P_2 and S_2 . An alternating current I_p is applied at frequency f (angular frequency $\omega = 2\pi f$) through the primary coils P_1 and P_2 , while the induced voltage ϵ_{ind} is measured across both the secondary coils S_1 and S_2 . The secondary coils are linked in the opposite direction in the circuit

such that the mutual inductances of each pair of primary and secondary coils – M_1 and M_2 , respectively – cancel in their contribution to the measured ϵ_{ind} when there is no sample inside coil S_1 . In ideal theory, the induced voltage is then proportional to χ_{eff} . In practice, the two pairs of coils are not identical which we account for with a small correction factor $\Delta M = M_1 - M_2$. Furthermore, there is a background voltage noise ϵ_{noise} measured when there is no sample and no applied current. The theory of induction allows derivation of an expression for the induced voltage ϵ_{ind}

$$\epsilon_{ind}^2 = \epsilon_{noise}^2 + \omega^2 I_p^2 [\alpha M_1 \chi_{eff} + \Delta M]^2. \quad (5)$$

where α is the fraction of volume of coil S_1 filled by the sample. This expression assumes that the background noise is distributed among all phases, which differs from the fixed phase of the induction signal, so that the root-mean-square values of the their respective contributions to the induced voltage are added in quadrature.

The geometric parameters of the system are as follows. The primary coil P_1 has length $L_p = 127.0 \pm 0.2$ mm, diameter $d_p = 50.8 \pm 0.2$ mm, and $N_p = 332 \pm 22$ turns of wire. The secondary coil S_1 has length $L_s = 25.4 \pm 0.2$ mm, diameter $d_s = 14.8 \pm 0.2$ mm, and $N_s = 190 \pm 14$ turns of wire. The coils S_2 and P_2 are nominally identical to S_1 and P_1 , respectively. All samples were prepared in cylindrical containers of length L that satisfies $L_s < L < L_p$ so that they were fully contained in the uniform region of the applied field and their edge effects have a minimal effect on the flux seen by coil S_1 . The filling fraction of the coil S_1 is then given by $\alpha = d^2/d_s^2$, where d is the diameter of the sample. We aligned the sample vertically within coil S_1 by finding the position of maximum measured induced voltage, as misalignment along the axis of the cylinder results in a reduced signal. The samples had inner diameter $d = 10.2 \pm 0.1$ mm unless otherwise specified, for aspect ratio corresponding to a typical filling factor $\alpha = d^2/d_s^2 = 0.471$. The sample aspect ratio is given by $\gamma_g = L/d$.

Here we summarize some typical electrical measurement parameter values and errors. We report root-mean-square values for all of our measurements of both alternating current and voltage throughout the paper. For our measurements, the applied alternating current is typically $I_p = 65 \pm 0.5$ mA (corresponding to an 0.8% error) unless otherwise noted, where the error is given by the manufacturer (Agilent model 34401A multimeter). We typically report measurements at frequencies f ranging from 200 to 2000 Hz, and χ_{eff} is calculated from Eq. 5, using an unweighted average over this frequency range unless otherwise specified. At these typical measurement values and when $\chi_{eff} \geq 1.2$, for example, we measure $\epsilon_{ind} \geq 23$ mV for different samples, with an uncertainty $\leq 0.2\%$ (≥ 0.05 mV) based on the $0.06\% \epsilon_{ind} + 0.04$ mV reported by the manufacturer, which is generally less than the uncertainty on the current measurement. The noise term ϵ_{noise} is due to electronic noise, and as such, varies when the measurement equipment is on. It is thus

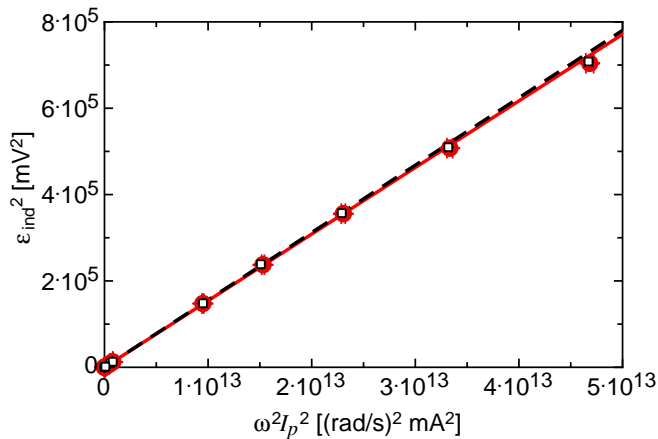


FIG. 2. Induced voltage from the mutual inductance of each pair of solenoid coils in isolation. Solid circles: coils P_1 and S_1 . Open squares: coils P_2 and S_2 . The slopes of the fits yield the squares of the mutual inductances M_1 (solid line) and M_2 (dashed line), used for calibration of the apparatus.

measured as ϵ_{ind} at a weak signal with frequency $f = 5$ Hz at $I_p = 65$ mA. We measured $\epsilon_{noise} = 3$ mV on average, with a standard deviation of 0.4 mV over the course of a series of experiments shown in one plot, or 1 mV over the longer time scale of different measurement series. When added in quadrature as in Eq. 5, this leads to an error on ϵ_{ind} of less than 0.2% for $\chi_{eff} \geq 1.2$ for example, which is small compared to the other errors for these typical measurement parameters. This error becomes dominant when the signal is smaller, notably where we test the linearity of the signal at small values of I_p or f in Sec. III A, or small ϕ where $\chi_{eff} \ll 1$. Similarly, the absolute error on χ_{eff} from the error of ΔM is 0.01, or equivalently less than 0.8% of $\alpha M_1 \chi_{eff}$ when $\chi_{eff} \geq 1.2$ for the typical measurement parameters (see Sec. II C on how values of M_1 and ΔM are obtained). Thus, the largest systematic source of error in calculating χ_{eff} from Eq. 5 unless otherwise noted typically comes from the 0.8% on the applied current I_p for our typical parameters and $\chi_{eff} \geq 1.2$.

When we repeated measurements by turning off the electronics, taking a sample container out from inside the coils, putting the sample back, and turn on the electronics again, the run-to-run standard deviation was 2.5% for suspensions and granular samples, and 0.2% for macroscopic solid pieces. The larger run-to-run variation of suspensions and powders may come from the rearrangement of particles as the sample containers are disturbed, but it is smaller than the 6% standard deviation observed in numerical simulations [11].

C. Inductance calibration

To provide calibration values of M_1 and ΔM in Eq. 5, we measure the mutual inductances of each coil inde-

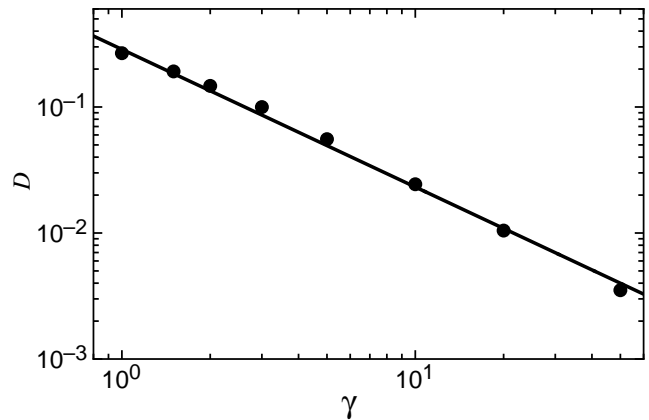


FIG. 3. Demagnetization factor D for a single-piece cylindrical sample as a function of aspect ratio. The data is reproduced from Chen et al. [15]. A power law is fit to obtain a reference curve to account for the demagnetization effect in our measurements.

pendently, in each case removing the other coil from the circuit and measuring without a sample. In these cases, the measured voltage is expected to be

$$\epsilon_{ind}^2 = \epsilon_{noise}^2 + \omega^2 I_p^2 M_i^2, \quad (6)$$

where $i = 1$ or 2 is the coil pair index number. Measurements of ϵ_{ind}^2 are shown as a function of $\omega^2 I_p^2$ in Fig. 2 for both coil pairs. We fit a linear function plus a constant to each to obtain the slopes M_1 and M_2 , respectively. The error bars in the figure represent the sum of a 0.2% standard deviation of multiple repetitions and a 0.8% systematic error. To obtain a fit with a reduced Chi-squared of 1 (where the reduced Chi-squared value of a fit corresponds to the mean-square difference between the data and fit, normalized by the error), we adjust the percentage input errors to 1.6% and 1.9% for coil pairs 1 and 2, respectively. The fit yields $M_1 = (1.245 \pm 0.004) \times 10^{-4}$ H and $M_2 = (1.253 \pm 0.004) \times 10^{-4}$ H. These measured values are consistent with the expected theoretical value $M = N_p N_s A_s / L_p = (1.2 \pm 0.1) \times 10^{-4}$ H based on the dimensions of the setup, where $A_s = \pi d_s^2 / 4$ is the cross-sectional area of the secondary coil. The difference between these measured mutual inductances is $\Delta M = M_2 - M_1 = (8 \pm 6) \times 10^{-7}$ H. These values M_1 and ΔM are used as calibrations to calculate χ_{eff} from Eq. 5.

D. Susceptibility calibration

We used single-piece solid cylindrical samples to calibrate χ_{eff} measurements in our setup. To account for the demagnetization effect, we use for reference a numerical simulation of the demagnetization factor D for single-piece cylindrical samples of various aspect ratios γ

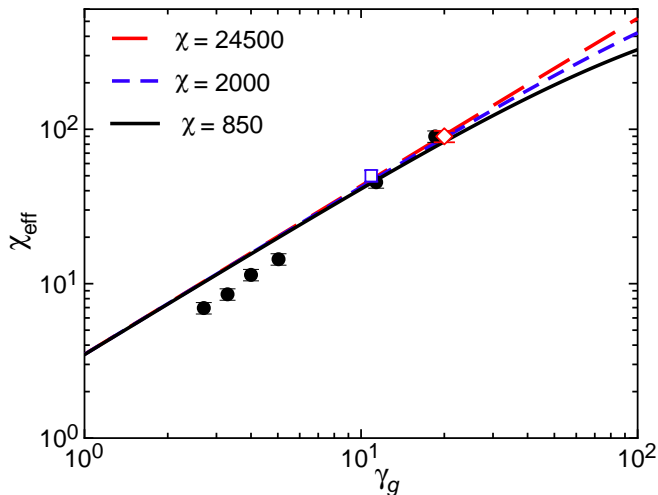


FIG. 4. Measured effective susceptibility χ_{eff} of single-piece solid samples as a function of aspect ratio γ . Solid circles: material susceptibility $\chi = 850$. Open square: $\chi = 2000$. Open diamond: $\chi = 24500$. Lines: fits of numerical simulation results from Chen et al. [15], for the different material susceptibilities χ as given in the legend to obtain reference curves χ_{ref} .

from Chen et al. [15], shown in Fig. 3. We fit the function

$$D = A\gamma^n. \quad (7)$$

to this data, over the range $0.7 < \gamma < 50$, which covers our measurement range. We adjusted the input error to be 8% to obtain a reduced Chi-squared of 1, yielding $A = 0.31 \pm 0.01$ and $n = -1.12 \pm 0.02$.

To calibrate our setup, we measured χ_{eff} of single-piece solid samples with different dimensions (the specific lengths and diameters are indicated in Fig. 5) and materials. Measured χ_{eff} are shown in Fig. 4 at different aspect ratios γ for ferrite ($\chi = 850$, Fair-Rite Products Corp.), mu-metal ($\chi = 2000$, Aperam), and Permalloy ($\chi = 24500$, National Magnetics Group, Inc.). The plotted errors are the sum of the 0.2% run-to-run variation and 0.8% systematic error. A reference curve χ_{ref} is shown in Fig. 4 for each material, which is calculated by inserting the fit function for D (Eq. 7) into Eq. 1 with $\phi = 1$. Since these χ are all much greater than 1, the predicted χ_{ref} curves are all close to each other. For aspect ratio $\gamma \geq 10$, the measured χ_{eff} values collapse onto the reference curves χ_{ref} within a root-mean-square difference of 7%. However, for $\gamma \leq 5$ the measured χ_{eff} are about 30% smaller than the reference curve.

To come up with an appropriate calibration adjustment, we first consider that sample aspect ratio may not be the primary parameter which it could depend on. In the ideal theory assumed in Eq. 5, if $L_s \ll L \ll L_p$, the magnetic field inside S_1 is expected to be uniform. In practice, fringe effects may add a correction. To come up with a calibration adjustment as a function of the sample length L , we replot our measurements of χ_{eff} for single-

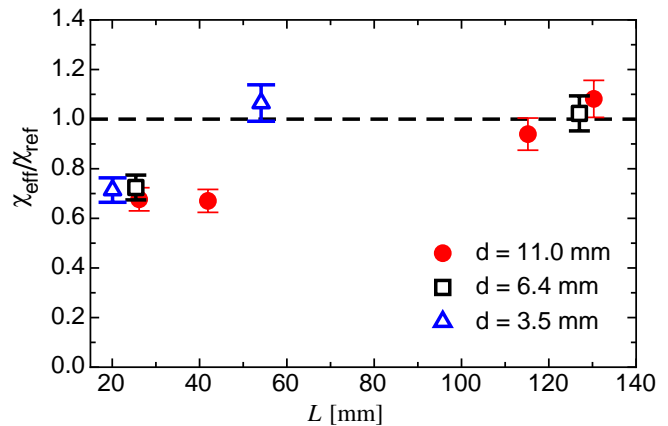


FIG. 5. Ratio between the measured effective susceptibility χ_{eff} for single-piece solid samples and the reference value from Chen et al. [15], as a function of sample length L . Sample diameters d are indicated in the legend. We adjust measurements of χ_{eff} for suspensions in later plots for $L < 50$ mm by a calibration factor based on this ratio.

piece samples from Fig. 4 normalized by the reference curve χ_{ref} as a function of the sample length L in Fig. 5. Different sample diameters d are indicated in the figure legend with uncertainties of 0.2 mm. A systematic dependence on L is observed in Fig. 5, similar to the trend in Fig. 4. In contrast, there is no systematic trend in d , as some points for each value of d are in each of the lower and upper ranges of χ_{eff}/χ_{ref} . This confirms the calibration should be made as a function of L , but not as a function of d . For $L \geq 54$ mm, the reference curve agrees with our measurement within a root-mean-square difference of 7% (a 7% error bar is plotted in Fig. 5 to see this). However, for $L \leq 42$ mm ($= 1.7L_s$), χ_{ref} is an average of $40\% \pm 4\%$ larger than χ_{eff} . Based on these results, we introduce a calibration factor in which the following measurements for χ_{eff} are shifted upwards by a factor of 1.4 for samples with $L \leq 42$ mm. We note that most of our samples in later measurements have $L \geq 54$ mm, and this calibration factor only needs to be applied to a few of our shortest samples, specifically for aspect ratio $\gamma_g = 2.5$ in Fig. 8, samples with $\gamma_g < 5$ in Fig. 9, and samples with aspect ratio $\gamma_g = 4.1$ in Figs. 13 and 14. Based on the variation of 7% around the reference curve observed here, we also introduce an error of 7% from unknown sources when comparing samples in all following measurements of χ_{eff} .

III. RESULTS

A. Linearity of magnetic response

To test the linearity of the magnetic properties of the materials with frequency, some examples of the measured susceptibility χ_{eff} are shown for dry granular materials

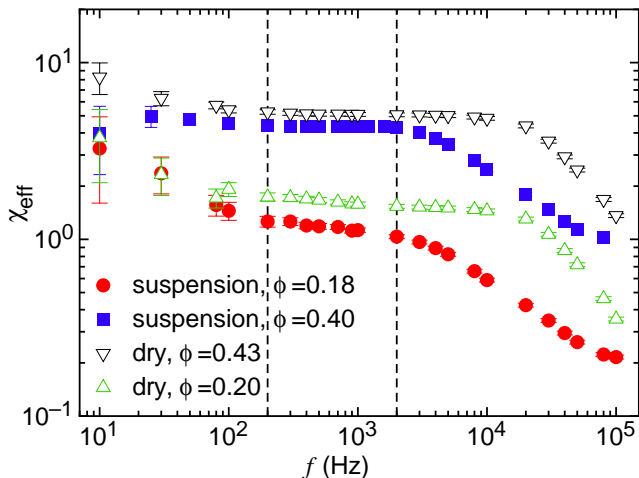


FIG. 6. Examples of χ_{eff} as a function of frequency f . Solid symbols: suspensions of iron particles in eGaIn at $\phi = 18\%$ (circles) and $\phi = 40\%$ (squares). Open symbols: dry granular materials at $\phi = 20\%$ (up-pointing triangles) and $\phi = 43\%$ (down-pointing triangles). χ_{eff} reaches a plateau for $f < 2000$ Hz. The vertical lines indicate the bounds of the frequency range where χ_{eff} is averaged over for measurements reported in other plots.

and suspensions as a function of frequency f in Fig. 6, at sample aspect ratio $\gamma_g = 11$, length $L = 112.2$ mm, and packing fractions ϕ shown in the legend. The error bars plotted the quadratic sum of the 2.5% run-to-run standard deviation and the 0.4 mV error on the noise voltage measurements, the latter of which tends to lead to a large error at low frequencies where the signal is weak. A plateau in χ_{eff} is found at frequencies $f < 2000$ Hz for all suspensions of nearly spherical particles reported in this paper. At higher frequencies, χ_{eff} decreases, qualitatively similar to the frequency response of other magnetic materials. The decrease starts at lower frequencies for suspensions than dry granular materials, which may be expected due to stronger eddy currents in the higher conductivity suspensions. At frequencies $f < 200$ Hz, the data remain consistent with the plateau, however there are large relative uncertainties in this range due to the low voltage signal. Thus, in other plots in this paper, we report the averaged χ_{eff} over the range of 200 Hz to 2000 Hz as the representative value for the low-frequency plateau, unless we specify otherwise that we found the low-frequency plateau in a different range. This could introduce an error if there is a trend in χ_{eff} with frequency, as seen for $\phi = 18\%$ suspension in Fig. 6. In this case, which is comparable to the worst case, using the mean of χ_{eff} for frequencies in the range of 200 Hz to 2000 Hz can underestimate a fit in the zero-frequency limit by up to 3%, which is negligible compared to the 7% error we use when comparing samples.

We next test whether the magnetic response is linear in the applied magnetic field H_{app} (equivalently, whether χ_{eff} is independent of H_{app}), and whether the suspen-

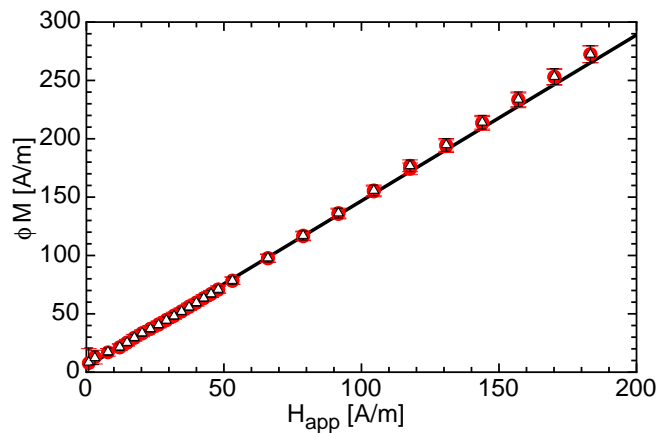


FIG. 7. Magnetization per unit volume of sample $\phi M = \chi_{eff} H_{app}$ of suspensions as a function of applied magnetic field H_{app} . Closed circles: increasing H_{app} (or I_p). Open triangles: decreasing H_{app} (or I_p). Line: linear fit. The suspension behaves as a linear paramagnetic material, with no hysteresis or significant remnant magnetization.

sions behave more like paramagnetic or ferromagnetic materials. We plot the magnetization per unit volume of sample $\phi M = \chi_{eff} H_{app}$ vs. the applied magnetic field $H_{app} = I_p N_p / L_p$ in Fig. 7 for a suspension with $\phi = 0.34$, $\gamma_g = 2.5$, and $L = 25.40$ mm. We performed these measurements with histories of both increasing and decreasing applied current I_p ($\propto H_{app}$). It is seen in Fig. 7 that these ramps give equivalent results, indicating a lack of hysteresis in the measured range. To test the linear response, we fit a linear function with a constant offset to these data where the random error is the quadratic sum of the 2.5% run-to-run standard deviation and the 0.4 mV random error on voltage measurements, which yields a reduced Chi-squared of 0.8. The consistency of the linear fit with the data confirms the data are consistent with a χ_{eff} independent of H_{app} over this range, verifying the linearity assumed in deriving Eq. 6. The error bars plotted in Fig. 7 include both these systematic and random errors. The constant offset in the linear fit was 5 A/m, which is consistent with $M = 0$ at $H = 0$ within the error of 12 A/m on M at that point due mainly to the 0.5 mA systematic error on the current, so there is no resolvable remnant magnetization. These properties suggest the suspensions behave as linear paramagnetic materials in this range, which is simpler for both modeling and control, despite the fact that the particles themselves are ferromagnetic. The suspensions are known behave like a ferrofluid such that after an applied magnetic field is removed, the particles separate and flow like a liquid [7]. This allows the ferromagnetic particles to move around in the liquid and reorient more freely than magnetic domains in a solid to avoid hysteresis and remnant magnetization.

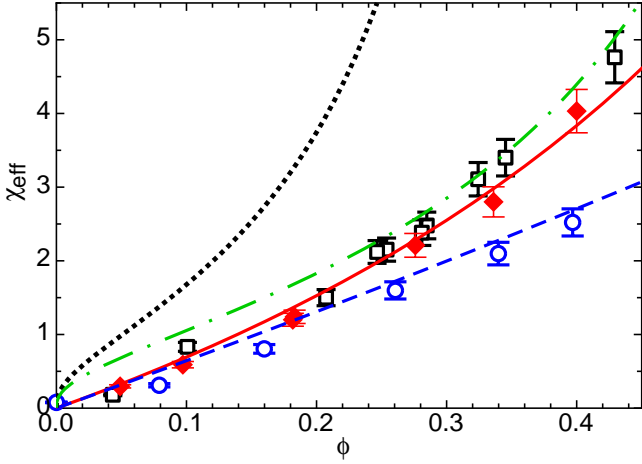


FIG. 8. Effective susceptibility χ_{eff} as a function of packing fraction ϕ for spherical particles ($\gamma_p = 1$). Squares: dry granular material, $\gamma_g = 11$. Diamonds: suspension, sample aspect ratio $\gamma_g = 11$. Circles: suspension, $\gamma_g = 2.5$. Suspensions exhibit a slightly smaller χ_{eff} than dry granular materials. Lines: fit of Eq. 8 for $\gamma_g = 11$ (solid line) and $\gamma_g = 2.5$ (dashed line), where fit parameters are obtained from simultaneously fitting data of Figs. 8, 9, and 10. Eq. 4 is shown for $\phi_c = 74\%$ (dashed-dotted line) and the measured liquid-solid transition $\phi_c = 40.7\%$ (dotted line). The divergence at the liquid-solid transition predicted by Eq. 4 is not observed in the measurements.

B. Variation of χ_{eff} with aspect ratios and packing fraction

Now that we have calibrated the apparatus and established linearity of the response over our measurement range, we now measure the dependence of the effective susceptibility χ_{eff} on the sample packing fraction ϕ , sample aspect ratio γ_g , and particle aspect ratio γ_p , to test and fit the model predictions of Eq. 3.

Figure 8 shows how χ_{eff} varies with packing fraction ϕ for two series of suspensions and one of dry granular materials with spherical particles ($\gamma_p = 1$), and sample aspect ratios $\gamma_g = 2.5$ and 11. Data at $\gamma_g = 2.5$ have been shifted upwards by a factor of 1.4 according to the calibration in Fig. 5. Measurements are made at packing fractions up to the liquid-solid transition $\phi_c = 40.7 \pm 0.3\%$ for the suspension, defined as the lowest packing fraction where a non-zero yield stress is measured. Measurements of the yield stress for these samples were reported in a previous paper [7]. For each series, χ_{eff} increases with increasing ϕ . On average, χ_{eff} of dry granular materials is higher than that of suspensions by 11% at the same ϕ .

Figure 9 shows the effective susceptibility χ_{eff} as a function of sample aspect ratio γ_g , for spherical particles ($\gamma_p = 1$) and $\phi = 40\%$. To vary γ_g and satisfy the condition $L_s < L < L_p$, the sample diameter d had to be varied along with the length. We use $d = 10.2 \pm 0.1$ mm for $\gamma_g < 15$, $d = 7.1 \pm 0.1$ mm for $\gamma_g = 19$, and

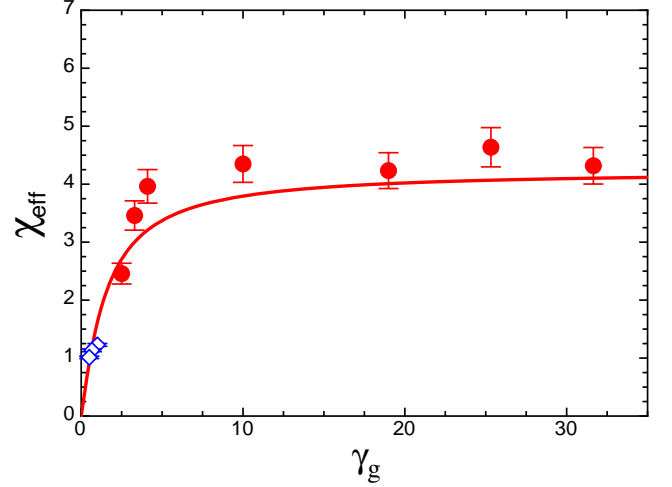


FIG. 9. Effective susceptibility χ_{eff} of suspensions as a function of sample aspect ratio γ_g . Solid symbols: spherical particles ($\gamma_p = 1$) at $\phi = 40\%$. Line: model result of Eq. 8, where fit parameters are obtained from simultaneously fitting data of Figs. 8, 9, and 10. Open Symbols: numerical simulation of spherical particles at $\phi = 40\%$ [11].

$d = 3.7 \pm 0.1$ mm for $\gamma_g > 22$. Measurements for $\gamma_g < 5$ have been adjusted upward by 40% according to the calibration in Fig. 5. At small γ_g , χ_{eff} increases with γ_g , and reaches a plateau for $\gamma_g \gtrsim 10$. For comparison to previous work in Fig. 9, we show numerical simulation results of randomly packed spherical particles at $\phi = 40\%$ [11] (Bjork et al. reported demagnetization factors D [11], which we converted to $\chi_{eff} = \phi/D$. Their aspect ratio was defined as the inverse of our aspect ratio definition.). The simulation data follow the same trend as ours.

To test the dependence of χ_{eff} on particle aspect ratio γ_p in Eq. 3 which assumes that particles are aligned with the applied magnetic field, we made dry samples of stacked cylindrical particles where the particles were forced to be aligned with the applied magnetic field. To make such aligned samples while holding γ_g and ϕ constant, we cut a 130 mm long cylindrical ferrite rod into collections of gradually smaller pieces to obtain a series of decreasing γ_p . Each piece was nearly cylindrical, with roughness on a scale of 1 mm at the two ends of the cylinder due to the cutting process. The packing fraction ϕ ranged from 100% to 97% due to some loss of material. This resulted in a number of pieces ranging from 1 for the largest γ_p to 32 for the smallest γ_p of the series. The pieces were arranged in a stack in the sample container with a common cylindrical axis aligned with the applied magnetic field. The measured χ_{eff} as a function of γ_p for these aligned particles is shown in Fig. 10 for two series, one with $\gamma_g = 20$ and one with $\gamma_g = 11$. χ_{eff} initially increases with increasing γ_p and levels off for larger γ_p .

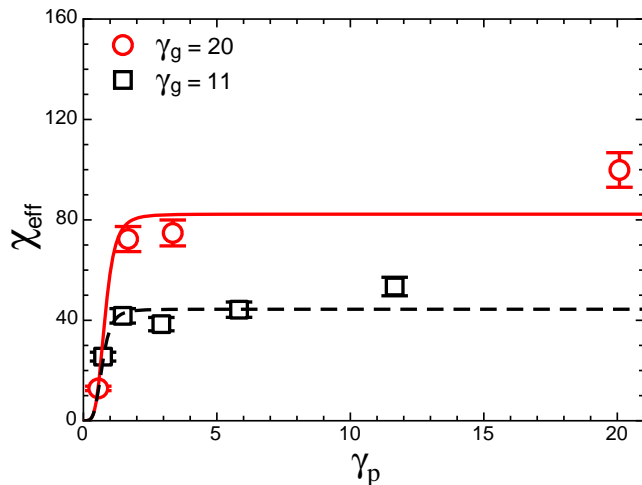


FIG. 10. Effective susceptibility χ_{eff} of suspensions of cylindrical rods forced to be aligned with the applied magnetic field as a function of particle aspect ratio γ_p , with $\phi \approx 100\%$. Values of γ_g are given in the legend. Lines: model result of Eq. 8 for $\gamma_g = 11$ (dashed line) and $\gamma_g = 20$ (solid line), where fit parameters are obtained from simultaneously fitting data of Figs. 8, 9, and 10. The simultaneous fits here and in Figs. 8 and 9 confirm the validity of Eq. 8 within a root-mean-square difference of 17%.

C. Testing the models for χ_{eff}

The measurements of χ_{eff} presented in Sec. III B over a wide range of packing fraction ϕ , sample aspect ratio γ_g , and particle aspect ratio γ_p now allow us to test the model of Eq. 3. In Eq. 3, the demagnetization factors D_g and D_p are unspecified functions of sample and particle geometry, respectively. While calculations have been made of D_g for some shapes [11], we are not aware of any model for D_p . To fit parameters, we assume that both D_g and D_p follow power laws of the form $D = A\gamma^n$ as shown in Fig. 3 for single-piece solid magnets [15]. Inserting this forms into Eq. 3 with different fit parameters for D_g and D_p yields our fit function

$$\chi_{eff} = \frac{\phi}{A_p \gamma_p^{n_p} (1 - \phi) + A_g \gamma_g^{n_g} \phi}. \quad (8)$$

We simultaneously least-squares fit all our suspension data in Figs. 8, 9, and 10 to Eq. 8 to obtain the fit parameters A_g , n_g , A_p , and n_p . Input error bars were adjusted to 17% to obtain a reduced Chi-squared of 1 from the fit. This indicates the model matches the data within a root-mean-square difference of 17%. Plots of Eq. 3 with these fit parameters are shown in Figs. 8, 9, and 10, where it is seen that the model captures the trends of χ_{eff} in ϕ , γ_g , and γ_p , respectively. The corresponding best fit parameters are $A_g = 0.4 \pm 0.1$, $n_g = -1.2 \pm 0.1$, $A_p = 0.16 \pm 0.01$, and $n_p = -4.4 \pm 0.3$. The best fit values of A_g and n_g are consistent with the fit values $A = 0.31 \pm 0.01$ and $n = -1.12 \pm 0.02$ from the data of Chen et al. [15] in

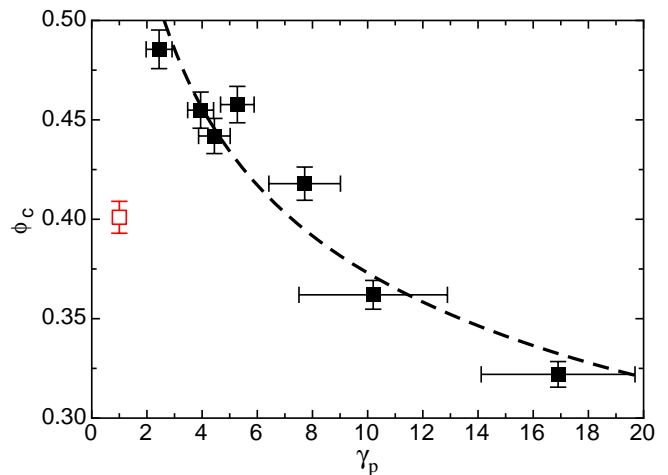


FIG. 11. Packing fraction of the liquid-solid transition ϕ_c as a function of particle aspect ratio γ_p . Solid symbols: suspensions of cylinders. Open symbol: suspension of spheres. Dashed line: power law fit to data for cylinders.

Fig. 3, confirming that D_g in Eq. 3 is consistent with the demagnetization factor D of individual particles [11].

To compare with the prediction of Martin et al. [12], we plot Eq. 4 as the dashed-dotted line in Fig. 8 with $\phi_c = 74\%$, the value used by Martin et al. [12]. The result using this value of ϕ_c happens to match well with our data with sample aspect ratio $\gamma_g = 11$. However, no sample aspect ratio dependence was prescribed in Eq. 4, and the model does not fit well to data at $\gamma_g = 2.5$. Furthermore, the value of ϕ_c suggested by Martin et al. [12] is unphysically large for a liquid-solid transition of a random arrangement of particles, where the particles just barely touch each other, which was the physical meaning of ϕ_c in Martin et al. [12]. Our suspensions have a liquid solid transition at $\phi_c = 40.7\%$, measured as the lowest packing fraction where the samples exhibit a non-zero yield stress like a solid [7]. To test the physical intent of that model, we plot Eq. 4 with $\phi_c = 40.7\%$ as the dotted line in Fig. 8. This prediction greatly overestimates our measurements, which do not exhibit the divergence at ϕ_c of the prediction. The lack of an observed divergence in χ_{eff} in the approach to ϕ_c is similar to simulations of dry granular materials [11].

D. Effect of particle misalignment

In the previous section, we tested the model of Eq. 3 for particles aligned with the applied magnetic field, which was an assumption of the model of Skomski et al. [1]. However, this is not a very practical case, as real suspensions of aspherical particles tend to have randomly arranged and oriented particles. To characterize how particle misalignment affects χ_{eff} , we made suspensions of cylindrical particles of various particle aspect ratios. We purchased iron wire (Goodfellow) and cut it to make

cylindrical particles with different particle aspect ratios γ_p . To obtain samples with enough particles to avoid significant finite size effects, while minimizing the number of cuts we needed to make, we used different wire diameters of 0.25, 0.5, and 1 mm, for samples with mean particle aspect ratio $\gamma_p > 10$, $5 \leq \gamma_p < 10$, and $\gamma_p < 5$, respectively. For samples of aspect ratio $\gamma_g = 4.1$ and length $L = 42$ mm, this results in the ratio of sample diameter to cylinder diameter between 17 and 9, and the ratio of sample diameter to mean particle length between 4.1 and 2.5, which is a range where the value of the packing fraction ϕ_c of the liquid-solid transition is within 4% of the infinite-size system limit [16, 17]. Effects of confinement on alignment are also presumed to be small in this system-size range. For example, in this range the partial particle alignment from this confinement changes the bulk rheology by less than 3% [17], but to our knowledge the effect on χ_{eff} from this confinement has not been characterized.

Before we compare χ_{eff} for particles of different aspect ratio γ_p , we first identify a meaningful packing fraction criteria for comparison. Since the packing fraction ϕ_c of the liquid-solid transition varies with γ_p [16, 17], it would not be meaningful to compare at the same absolute packing fraction. Rather, we chose to measure χ_{eff} at a fixed relative packing fraction ϕ/ϕ_c near the liquid-solid transition to determine the maximum χ_{eff} we would expect to obtain in the liquid phase for each γ_p . Assuming χ_{eff} increases monotonically with ϕ up to ϕ_c for any particle shape as seen for spheres in Fig. 8, this would be the packing fraction where χ_{eff} is maximized for each particle shape, and any lower value of χ_{eff} could be obtained by tuning the packing fraction down to an appropriate value. ϕ_c was measured for each γ_p by observing the change in surface reflectivity as the particles poked through the liquid-air interface of the suspension when $\phi > \phi_c$ [18]. This transition is sharp and easily observed, allowing us to measure it with an uncertainty on ϕ_c of $\pm 1\%$. ϕ_c is plotted as a function of particle aspect ratio γ_p in Fig. 11. The horizontal error bars indicate the standard deviation of particle aspect ratios due to the variation in cut particle lengths. The measured ϕ_c decreases with increasing γ_p for cylinders, consistent with previous results [19]. For later input into models, a power law is fit to ϕ_c for cylinders, yielding $\phi_c = 0.62\gamma_p^{-0.22}$. For comparison we also plot ϕ_c for the spherical particles used in earlier sections in Fig. 11. The value of ϕ_c for the spheres do not follow the same trend as the cylinders, not only because of the particle shape, but also the different material source may subtly affect interparticle interactions that can have a significant affect on ϕ_c [20].

Since sample preparation procedures can affect the alignment of particles, we also characterize the tendency for the particles to align based on different shaking procedures after the sample was loaded into the cell, but before the magnetic field was applied. We use a suspension with sample aspect ratio $\gamma_g = 4.1$, sample length $L = 42$ mm, and particle aspect ratio $\gamma_p = 5.3$, at a

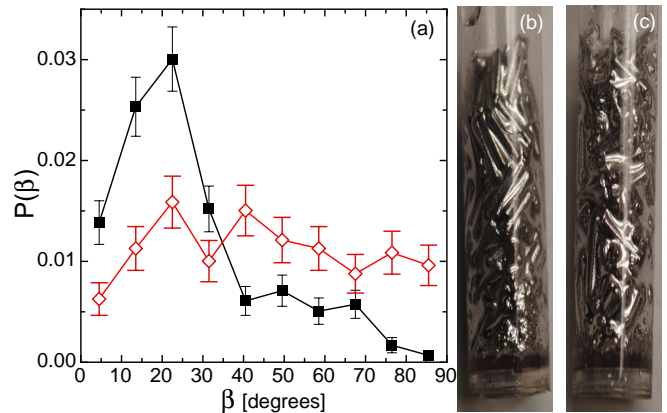


FIG. 12. (a) Probability distribution of particle alignment angles β relative to the applied magnetic field, for samples with length $L = 42$ mm, sample aspect ratio $\gamma_g = 4.1$, particle aspect ratio $\gamma_p = 5.3$, and packing fraction $\phi/\phi_c = 1.02$. Solid squares: samples were shaken along the axis of the cylindrical tube to partly align the particles with the external magnetic field. Open diamonds: samples were shaken using a vortex mixer, resulting in a more random alignment. Pictures of the samples for the 2 shaking procedures are shown in panels (b) and (c), respectively, where the applied magnetic field is aligned in the vertical direction.

packing fraction $\phi/\phi_c = 1.02$. This packing fraction is just barely resolvable to be above the liquid-solid transition, so we can observe the alignment of the particles as they poke out the liquid-air interface. In one case, samples were shaken along the axis of the cylindrical tube to partly align the particles with the external magnetic field, shown in Fig. 12b. In a second case, the same samples were shaken with a combination of linear and rotational shaking (Vortex Genie 2), resulting in a more random alignment, shown in Fig. 12c for the same sample parameters. Note the alignment in the bulk could be quantitatively different from value based on the particles at the boundary, so these pictures at the surface of the sample should be taken as a coarse characterization of the alignment of particles. These images were analyzed to measure the angle β of each particle relative to the applied magnetic field, which was aligned with the cylindrical tube axis. Figure 12a shows the probability distribution $P(\beta)$ for both of these samples. For samples shaken by the vortex mixer, we observe a relatively flat distribution, with a mean $\langle \beta \rangle = 44.7^\circ$ corresponding to a random alignment. Samples shaken along the axis direction, while still fairly random, display a preferred alignment angle $\beta = 20^\circ$, and a mean $\langle \beta \rangle = 27.3^\circ$, corresponding to better alignment with the applied magnetic field at $\beta = 0^\circ$.

Now that we have identified appropriate packing fractions to compare samples, and characterized the amount of alignment from different preparation procedures, we can systematically test trends in effective susceptibility χ_{eff} as a function of particle aspect ratio γ_p for suspen-

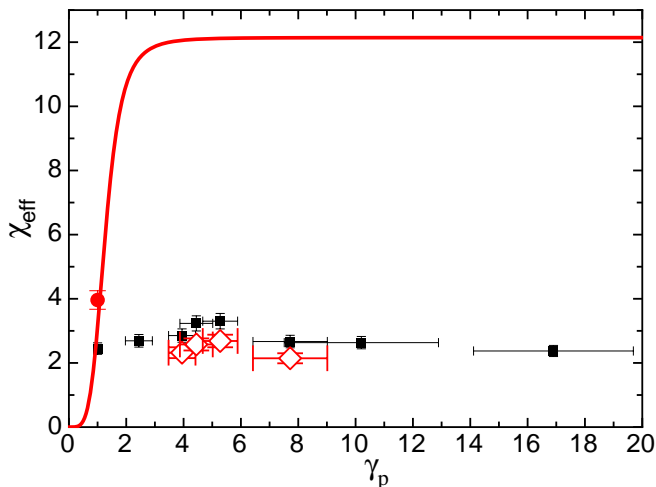


FIG. 13. Effective susceptibility χ_{eff} as a function of particle aspect ratio γ_p , at $\gamma_g = 4.1$ and $\phi/\phi_c = 1.02$. Solid squares: samples were shaken beforehand along the axis of the tube to partly align the particles with the external magnetic field. Open diamonds: samples were shaken beforehand using a vortex mixer, resulting in a more random alignment. Solid circle: random packing of spheres ($\gamma_p = 1$), which cannot align. Solid line: model of Eq. 8. The model overestimates χ_{eff} by about a factor of 4 for suspensions that are not aligned with the external magnetic field.

sions of randomly arranged particles. The measured χ_{eff} is shown as a function of γ_p in Fig. 13, at a fixed relative packing fraction $\phi/\phi_c = 1.02$, $\gamma_g = 4.1$, $L = 42$ mm, and for both shaking procedures. The error bars on γ_p indicate the standard deviation of the aspect ratio due to the distribution of particle lengths in each sample.

To test how the model developed for particles aligned with the applied magnetic field applies to randomly arranged particles, the model prediction of Eq. 8 is shown in Fig. 13, where we use the fit parameter values obtained from the simultaneous fit of data in Figs. 8, 9, and 10, and the power law fit expression for ϕ_c from the fit in Fig. 11 in place of ϕ in Eq. 8. The model overestimates χ_{eff} by about a factor of 4 in this case where the particles are not aligned with the applied magnetic field. Since that model fit well to data for aligned particles, this indicates the random alignment severely reduces χ_{eff} . χ_{eff} is comparable to the value for spheres, which suggests the demagnetization effect may be about as significant for randomly arranged long cylinders as it is for spheres. The much larger χ_{eff} obtained in Fig. 10 for large γ_p is apparently possible only because the strict alignment of the particles with the applied magnetic field reduces the demagnetization effect. The trend of higher χ_{eff} with better aligned particles is also seen in our samples with different shaking procedures: the better aligned particles that were shaken along the cylinder axis had a consistently 20% higher χ_{eff} than the more randomly arranged particles that were shaken by the vortex mixer. A simple

quantitative estimate of the average vector component of alignment $\cos\langle\beta\rangle$ is also 20% higher for the particles shaken along the cylinder axis than those shaken by the vortex mixer. It suggests, at least in the ballpark, the decrease of χ_{eff} in Fig. 13 may be associated with the change in particle alignment for these two samples of randomly arranged particles. However, extrapolating this simple estimate does not reach the model of Eq. 8, which suggests that much better alignment would be needed to reach that regime than is likely to be obtained in suspensions with even partially randomly arranged particles, regardless of shaking or other procedures used to get a preferential alignment.

While there is little trend in χ_{eff} over the range of γ_p measured in Fig. 13, it is notable that χ_{eff} exhibits a local maximum in γ_p . In contrast, Eq. 8 predicts χ_{eff} to be a monotonically increasing function of γ_p (as seen in Fig. 10). This local decrease in χ_{eff} with γ_p is not due to the different wire diameters used, as in the range $5 \leq \gamma_p < 10$ where χ_{eff} decreased, the same diameter wires were used. Similarly, finite-size effects cannot explain the peak, as the number of particles is decreasing over the same range of γ_p , which would only be expected to produce more alignment and a larger χ_{eff} , in contradiction to the trend observed in χ_{eff} . It could also be proposed that the local peak in $\chi_{eff}(\gamma_p)$ could be due to a competition between the increasing χ_{eff} in Eq. 8 and the decreasing ϕ_c with γ_p . However, as shown in Fig. 13, the model of Eq. 8 still has no local maximum in this parameter range – even when accounting for this decreasing ϕ_c with γ_p . This insensitivity to ϕ in the model is apparent in the limit of large γ_p of Eq. 3, which becomes $\chi_{eff} \approx 1/D_g$, independent of ϕ . The cause of this local maximum in $\chi_{eff}(\gamma_p)$ remains unknown.

The data in Fig. 13 were taken at $\phi/\phi_c = 1.02$, corresponding to a jammed state where particles were not free to realign in the applied magnetic field. If instead particles were at a lower packing fraction in a liquid state, they might be expected to be able to more freely and better align with the applied magnetic field to reach the higher χ_{eff} predicted by Skomski et al. [1]. To test this hypothesis, we measured χ_{eff} as a function of packing fraction ϕ , for 0.5 mm diameter wire cut to length 3.2 mm with a standard deviation of 0.6 mm to obtain a particle aspect ratio $\gamma_p = 6.3 \pm 1.3$, near the peak found in Fig. 13. We started with a sample aspect ratio of $\gamma_g = 4.1 \pm 0.3$ at $\phi = 0.42$ in a 10.2 mm diameter tube, and diluted the sample with more liquid to increase ϕ . The sample aspect ratio decreased to 3.8 as the liquid-solid transition was crossed as the suspension packed more efficiently, without trapped air. Upon further dilution, the sample aspect ratio increased in inverse proportion to the packing fraction due to the increase in liquid volume. Because the signal was weaker at these lower frequencies, the calibration of ϵ_{noise} was done with more precision by measuring induced voltage separately before each data point with the current source outputting at the frequency and applied current of the data point but without a sample.

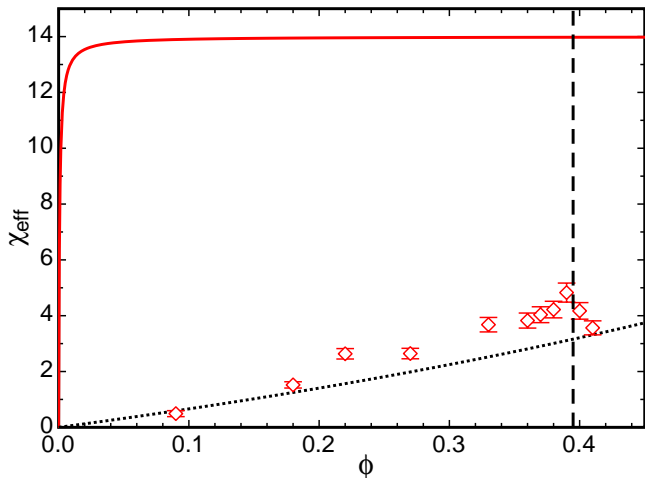


FIG. 14. Effective susceptibility χ_{eff} as a function of packing fraction ϕ for particle aspect ratio $\gamma_p = 6.3$ cylinders. Solid line: model of Eq. 8 for $\gamma_p = 6.3$. Dotted line: model of Eq. 8 for spheres ($\gamma_p = 1$). Vertical dashed line: the packing fraction of the liquid-solid transition. The model still overestimates χ_{eff} by a factor of 3 or more for suspensions of randomly aligned cylinders, regardless of whether they are in a liquid or solid state.

The plateau where χ_{eff} was independent of frequency occurred for $f < 200$ Hz for these cylinders, so the reported χ_{eff} was obtained from a weighted average of data in that range.

Values of χ_{eff} for these particle aspect ratio $\gamma_p = 6.3$ cylinders are shown as a function of packing fraction ϕ in Fig. 14. We only report χ_{eff} for samples shaken in the vortex mixer, as samples shaken vertically to intentionally align particles showed an increase in χ_{eff} of typically 20%, as found in Fig. 13. For $\phi \geq 0.33$, the samples had length $L < 42$ mm, so measured χ_{eff} values were scaled up by a factor of 1.4 according to the calibration in Sec. IID. χ_{eff} increases with ϕ for cylinders as it does for spheres for $\phi < \phi_c$. We do find a decrease in χ_{eff} as ϕ increases above ϕ_c , as expected due to the inability of particles to rearrange for $\phi > \phi_c$. The prediction of Eq. 8 for aspect ratio $\gamma_p = 6.3$ is shown as the solid line in Fig. 14. The prediction is again well above the data, by a factor of 3 or more. A correction for the variation of sample aspect ratio γ_g from the dilution according to Eq. 8 would not increase χ_{eff} by more than 10% for any data point, not nearly enough to match the prediction shown in Fig. 14. For comparison, we also plot the prediction of Eq. 8 for aspect ratio 1 as the dotted line in Fig. 14. The aspect ratio $\gamma_p = 6.3$ particles do have a slightly higher χ_{eff} than spheres, and reach up to $\chi_{eff} = 4.8$ at the highest packing fraction of the liquid state ($\phi = 0.39$). However, the disagreement with prediction confirms that even in the liquid state, the larger χ_{eff} predicted by Skomski et al. [1] is not realized, due to the random arrangement and orientation of particles in suspension which produces a strong demagnetization

effect even for large particle aspect ratios.

IV. CONCLUSIONS

In this paper, we reported measurements of the effective magnetic susceptibility χ_{eff} of suspensions as a function of packing fraction ϕ , sample aspect ratio γ_g , and particle aspect ratio γ_p . When particles are aligned with the applied magnetic field, the model of Skomski et al. [1] can be fit with power laws for the demagnetization factors D_g and D_p describing the aspect ratio dependence of the sample and particles, respectively, in the form of Eq. 8 with a root-mean-square difference of 17%. This was done by simultaneously varying the three model parameters over the range $0 \leq \phi \leq 40.7\%$ (up to the liquid-solid transition ϕ_c), $2.5 \leq \gamma_g \leq 32$, and $1 \leq \gamma_p \leq 20$. This indicates the model which was originally derived for ellipsoids can be approximately applied to other shapes, in particular cylinders. This fit yields $D_g = 0.4\gamma_g^{-1.2}$, consistent with values obtained for single-piece solids over a smaller parameter range [15], and $D_p = 0.16\gamma_p^{-4.4}$ to characterize the particle aspect ratio dependence for the first time, to our knowledge. However, for non-spherical particles randomly oriented in suspensions, the model prediction overestimates the measurements by a factor of 4 for $\gamma_g = 4.1$. As a result of these lower values of χ_{eff} for randomly aligned cylinders, we find χ_{eff} to be only 20% higher for aspect ratio $\gamma_p = 6.3$ cylinders than spheres. This effect from particle misalignment remains to be included in models. The largest effective susceptibility we found was $\chi_{eff} = 4.8$ for cylinders of particle aspect ratio $\gamma_p = 6.3$ and sample aspect ratio $\gamma_g = 4.1$. We also observed that $\chi_{eff}(\gamma_p)$ displays a local maximum at $\gamma_p \approx 5$ for $\gamma_g = 4.1$. This feature is unexpected, as it was predicted that the maximum χ_{eff} would increase monotonically with γ_p [1]. Another prediction that χ_{eff} would diverge to approach the material susceptibility χ at the liquid-solid transition ϕ_c [12] fails dramatically, as we observe only $\chi_{eff} \approx 4$ in the limit of this transition.

This failure to achieve the predicted χ_{eff} approaching χ for large packing fraction and/or large aspect ratio may limit applications of magnetic suspensions, as $\chi_{eff} \approx \chi$ would have allowed for much stronger magnetic responses of suspensions, comparable to ferromagnetic materials. Nonetheless, we do find a significant range of tunable magnetic properties of magnetic suspensions up to $\chi_{eff} \approx 4$ for spherical particles, several orders-of-magnitude stronger than other paramagnetic fluids, which typically have χ in the range of 10^{-9} to 10^{-4} . The linearity of the magnetic response without hysteresis, like paramagnetic materials, can also be desirable for simple control.

V. ACKNOWLEDGMENTS

We thank Ethan Kyzivat for helping out with preliminary experiments, and acknowledge financial support from

NSF Grant No. CBET-1255541 and AFOSR FA 9550-14-1-0337.

-
- [1] R. Skomski, G. C. Hadjipanayis, and D. J. Sellmyer, *IEEE transactions on magnetics* **43**, 2956 (2007).
- [2] R. E. Rosensweig, *Ferrohydrodynamics* (Courier Corporation, 2013).
- [3] J. de Vicente, D. J. Klingenberg, and R. Hidalgo-Alvarez, *Soft Matter* **7**, 3701 (2011).
- [4] R. Monchaux, M. Berhanu, M. Bourgoïn, M. Moulin, P. Odier, J.-F. Pinton, R. Volk, S. Fauve, N. Morandant, F. Pétrélis, A. Chiffaudel, F. Daviaud, B. Dubrulle, C. Gasquet, L. Marié, and F. Ravet, *Physical Review Letters* **98**, 044502 (2007).
- [5] R. Stieglitz and U. Müller, *Physics of Fluids* **13**, 561 (2001).
- [6] A. Gailitis, O. Lielausis, S. Dement'ev, E. Platcis, A. Ciferons, G. Gerbeth, T. Gundrum, F. Stefani, M. Christen, H. Hanel, and G. Will, *Physical Review Letters* **84**, 4365 (2000).
- [7] F. Carle, K. Bai, J. Casara, K. Vanderlick, and E. Brown, *Phys. Rev. Fluids* **2**, 013301 (2017).
- [8] A. Aharoni, *Journal of Applied Physics* **83**, 3432 (1998).
- [9] J. de Vicente, F. Vereda, J. P. Segovia-Gutiérrez, M. d. P. Morales, and R. Hidalgo-Ivarez, *Journal of Rheology* (1978-present) **54**, 1337 (2010).
- [10] B. Bleaney and R. A. Hull, *Proceedings of the Royal Society of London A: Mathematical, Physical and Engineering Sciences* **100**, 100 (1922).
- [11] R. Bjørk and C. R. H. Bahl, *Applied Physics Letters* **103**, 102403 (2013).
- [12] A. Martin, P. Odier, J.-F. Pinton, and S. Fauve, *The European Physical Journal B - Condensed Matter and Complex Systems* **15**, 151001 (2002).
- [13] P. Frick, S. Khripchenko, S. Denisov, D. Sokoloff, and J.-F. Pinton, *The European Physical Journal B - Condensed Matter and Complex Systems* **15**, 151002 (2002).
- [14] M. D. Dickey, R. C. Chiechi, R. J. Larsen, E. A. Weiss, D. A. Weitz, and G. M. Whitesides, *Adv. Funct. Mater.* **18**, 1097 (2008).
- [15] D. X. Chen, E. Pardo, and A. Sanchez, *Journal of Magnetism and Magnetic Materials* **306**, 135 (2006).
- [16] K. W. Desmond and E. R. Weeks, *Phys. Rev. E* **80**, 051305 (2009).
- [17] E. Brown, H. Zhang, N. A. Forman, B. W. Maynor, D. E. Betts, J. M. DeSimone, and H. M. Jaeger, *J. Rheology* **54**, 1023 (2010).
- [18] E. Brown, H. Zhang, N. A. Forman, B. W. Maynor, D. E. Betts, J. M. DeSimone, and H. M. Jaeger, *Physical Review E* **84**, 031408 (2011).
- [19] A. P. Philipse, *Langmuir* **12**, 1127 (1996).
- [20] V. Trappe, V. Prasad, L. Cipelletti, P. N. Segre, and D. A. Weitz, *Nature* **411**, 772 (2001).